Partial Discharge-Based Ageing Assessment of High Voltage Crosslinked Polyethylene Cable

S. H. Sulaiman[1*], A. Abdulkarim[1,2], A. S. Abubakar[1], G. S. Shehu[1], U. Musa[1], A. A. Mas'ud[3]

[1]Department of Electrical Engineering, Ahmadu Bello University, Zaria, Nigeria.
[2]Department of Electrical, Telecommunication and Computer Engineering, Kampala International University, Kampala, Uganda.
[3]Department of Electrical Engineering, Jubail Industrial College, Jubail, Kingdom of Saudi Arabia.

ABSTRACT: High Voltage (HV) cables are important components of modern power transmission and distribution networks. However, the reliability of such networks depends, to a large extent, on the health condition of the cables. The presence of voids within the insulation materials which could arise from overstressing, manufacturing defects as well as poor workmanship enhances the electric field within and around the defect which can lead to the occurrence of partial discharges (PDs). Furthermore, severe PD activity can deteriorate the cable dielectric material and cause accelerated asset ageing. Also, experimental monitoring of cable networks is expensive and time-consuming. Hence, in this research, a three-dimensional (3D) finite element model (FEM) of a crosslinked polyethylene (XLPE) cable was simulated in COMSOL Multiphysics software environment to analyse the behaviour of electric field in healthy and defective cable under different cavity sizes and applied voltages. The electric field magnitude at the centre of a 1.0 mm air void was recorded to be 2.539 kV/mm, representing a 24.07% increase over that of the corresponding healthy cable, 2.9539 kV/mm. PD activity was also studied using COMSOL Multiphysics software alongside MATLAB software environment by adopting free parameters corresponding to three ageing phases of the cable obtained from experiments for 50 cycles of the applied voltage. The results show that PD repetition frequency increases as the cable ages, resulting in 9.82, 15.82, and 17.20 PDs per cycle for ageing stages 1, 2, and 3 respectively.

KEYWORDS: Ageing, Cable, Electric Field, Finite Element Analysis, PRPD Patterns

[Received Feb. 5, 2024; Revised Nov 10, 2024; Accepted Nov 29, 2024] Print ISSN: 0189-9546 | Online ISSN: 2437-2110

LIST OF ABBREVIATIONS

2D	Two-Dimensional	ICC	Induced Charge Concept
3D	Three-Dimensional	MATLAB	Matrix Laboratory
AC	Alternating Current	P	Cavity pressure
DC	Direct Current	PD	Partial Discharge
FEA	Finite Element Analysis	PRPD	Phase Resolved Partial Discharge
FEM	Finite Element Method	PSA	Pulse Sequence Analysis
HV	High Voltage	XLPE	Crosslinked Polyethylene

I. INTRODUCTION

Power cables are used extensively in the transmission and distribution of electric power at various voltage levels. They have the advantage of long lifespan and high current carrying capacity. However, the performance of power cables is affected by insulation defects such as air voids, cracks, and contaminations which might be inherent from the point of manufacturing or arising from poor workmanship (Arikan *et al.*, 2023; Fikri and Abdul-Malek, 2023). The electric field within the cable, which is expected to be uniformly distributed under normal conditions, becomes concentrated at the location of the defects making the area under high stress and vulnerable to partial discharge (PD). A severe PD activity can lead to accelerated cable ageing and its eventual failure before the expected end of life (Boudiaf *et al.*, 2022). PD is a physical phenomenon that involves conduction through electrically weak points such as gaseous inclusions in insulation but does not completely bridge the gap between the electrodes. Hence, it is imperative to analyse the behaviour and distribution of the electric field in the model both under normal operation conditions and after PD occurrence.

*Corresponding author: shsulaiman@abu.edu.ng

doi: http://dx.doi.org/10.4314/njtd.v21i4.2351

PD occurrence is one of the electrical stresses identified to harm cable operation and its overall lifespan (Aliyu *et al.*, 2023). Thus, its continuous measurement is needed for predicting the time to failure of the cable. Classical PD measurement through an experimental approach is expensive, noise-prone, and mostly involves the destruction of the cable section. Hence, simulation models were considered as an alternative approach. Two popular approaches namely phase-resolved partial discharge (PRPD) and pulse sequence analysis (PSA) are used to represent PD behaviour in a dielectric (Dmitriev *et al.*, 2023). According to (Illias, Yuan*, et al.*, 2012) both analyses may be used in distinguishing the three basic types of PDs (surface, internal, and corona). However, statistical properties of the PD activities can be obtained from PRPD with loss in sequence while in PSA only the PD sequence may be obtained but not the statistical data (Illias, Chen*, et al.*, 2012).

Cable ageing, like other power systems assets, obeys the Bathtub Curve (Choudhary *et al*., 2024) which has three distinct phases namely the 'burn-in phase', 'the useful life phase', and 'the wear-out phase'. Early failures are usually due to manufacturing imperfections, poor workmanship as well as third-party damages. In the second stage, component wear-out, environmental stress, and several other factors are responsible for asset failures. As time progresses, into the third phase, the bulk dielectric strength degrades due to events such as water ingress and detachments at material interfaces, raising local stress. The net effect of these reactions is referred to as ageing. Hence, ageing is the rate at which equipment degrades and approaches its end of life. Ageing in HV cables depends on many factors such as voltage stress, thermal stress, maintenance strategy, age, and environment (Mirshekali *et al,* 2024).

Cable ageing is generally assessed using either electrical, mechanical, or thermal approaches or a combination of them (Mirshekali *et al.*, 2024). However, the electrical assessment was identified to be the most widely used due to the adverse effects caused by electrical stresses such as partial discharges (Mas'ud *et al.*, 2022) followed by thermal stress. The most prominent electrical property used in the assessment of cable ageing is the PD caused mostly due to the concentration of electric fields at the defect sites (Arikan *et al.*, 2023; Polyakov *et al.*, 2018). Due to their significant degradation impact, thermal and electrical stress-based ageing models are discussed here.

A. Electrical Ageing Models

Electrical ageing occurs as a result of free electrons and charge carriers that are present due to an enhanced electric field. These free electrons, at low concentrations, collide rapidly with the dielectric molecules and ionize them. The collision liberates additional free electrons at high concentrations leading to an avalanche that causes current flow (Choudhary *et al.*, 2022). Electrical overstress may give rise to the accumulation of space charge and the inception of PDs and electrical trees within defects. Hence, electrical ageing models are based on such stress markers (Liu *et al.*, 2012).

B. Thermal Ageing Models

Thermal ageing involves the degradation of an HV cable due to a rise in temperature within the insulation and in the cable's surrounding environment. Thermal stress produces irreversible and enduring reactions that eventually affect the insulation properties and increase the dissipation factor. These models are mostly based on the Arrhenius equation (Bessissa *et al.*, 2017).

In this paper, a 3-dimensional XLPE cable model corresponding to that of (Musa *et al*., 2021) was simulated in the COMSOL Multiphysics software environment. The two results were compared and further analysis of the effect of cavity size and magnitude of stressing voltage was performed on the 3D cable model in this work. PD analysis was also investigated in three ageing stages of the cable. An efficient method of monitoring the electrical ageing progress of power cables through the use of PRPD patterns derived from the 3-dimensional FEM cable model is the main contribution of this paper. The continuous monitoring of the state of HV assets will help utilities to prepare ahead and take proper measures to ensure a reliable power supply to the consumers and at the same time save cost.

II. LITERATURE REVIEW

Analysis of electric field as well as PD activity using a 2-dimensional FEA approach has been well reported in the literature. Illias *et al.*,(2011) proposed a 2D FEA model for a spherical air void that was used to study the impact of the void size on the electric field as well as the resulting PD activity. Khouildi *et al.*, (2016) employed COMSOL Multiphysics and analysed how different defects affect the operation and field distortion in an XLPE cable when considered separately and cumulatively. The maximum field strength increases with void size and decreases as the defect position is moved away from the HV electrode in all three cases considered. Uydur *et al.*, (2018) investigated how three different types of defects having the same sizes affect the distribution of electric field in two similar cables with different conductor cross-sectional areas using the 2D FEM approach. The field distribution was analysed at three locations within the insulation and near the ground electrode.

The performance of FEA and the induced charge concept (ICC) of PD modelling was compared by Borghei *et al.*, (2020) under variations of internal pressure, geometry, and the cavity dimension in an epoxy resin insulation. PRPD patterns were used to present the results of both methods. the work shows the superiority of the FEA over ICC in terms of PD repetition frequency, maximum real charge, and mean apparent charge magnitudes. A 2D model of a single core medium voltage XLPE cable under an AC voltage stress of 11 kV amplitude and frequency of 50 Hz was presented in (Musa *et al.*, 2021). Electric field distribution within the cable model was analysed for healthy cable and the defective ones containing a single air void. The authors obtained an increased average cavity field of 27.1% for the defective cable over the healthy one. This model was equally employed by Musa *et al.*, (2023) to study the

ageing progression of an HV cable due to PD activity in a single air cavity within the insulation.

It is evident that, over the years, researchers employed 2D FEA models to assess cable ageing in the presence of spherical voids. However, the defect is approximated to be cylindrical with uniform cross-sectional area in those models. Hence, a 3-dimensional approach that captures the exact geometry of the spherical void will enhance the accuracy of the electric field and PD charge magnitude estimation.

III. METHODOLOGY

In this research, an electrical ageing assessment of a crosslinked polyethylene (XLPE) cable based on the generation of PRPD patterns and the associated PD charge magnitudes was employed. The method involves building an FEA 3D model of a single core XLPE cable in a COMSOL Multiphysics software environment and simulated under an 11kV, 50 Hz AC voltage excitation. The electric field distribution was then analyzed at different cavity sizes and stress voltage magnitudes and compared with those reported by (Musa *et al.*, 2021) for a 2D model of the corresponding cable. Also, PD simulation was performed for different ageing stages of the cable to ascertain the trend of PRPD patterns in each ageing stage and determine the extent to which continuous PD activity affects the overall ageing process of the cable. The single-core cable has six (6) layers including a copper core, while the insulation material is XLPE screened from the conductor and the ground through graphite layers. The cable's electrical properties and the geometrical specifications are adopted from the study by Musa *et al.*, (2023) and presented in Tables 1 and 2 respectively.

Table 1. Material Properties of the Adopted Cable

Material	Conductivity (S/m)	Relative Permittivity
Copper	5.85×10^{7}	1
Aluminum	3.57×10^{7}	2.2
XLPE	1.0×10^{-15}	2.3
Graphite	3.0×10^{-3}	500
PVC	1.0×10^{-15}	2.9
Air	1.0×10^{-100}	1

Table 2. Geometry of the Adopted XPLE Cable

Layer	Component	Material Type	Value (mm)
1	Conductor radius	Aluminum	3.50
2	inner sheath thickness	Graphite	0.50
3	Insulation thickness	XLPE	5.50
4	Insulation screen thickness	Graphite	0.50
5	Armor wire thickness	Steel	0.65
6	Outer sheath thickness	XLPE	2.00
	Overall cable radius	-	12.65

A. Electric Field Analysis

A 3D model of the cable was simulated in COMSOL Multiphysics software environment using the finite element method (FEM) technique to analyse the distribution of electric field in and around the single air void contained in the cable insulation. Electric field distribution along the 3D cutline which emanates from P_1 (x_1 = 2.839 mm, y_1 = 2.829 mm, z_1 = 10.0 mm) which dissects the cavity and terminates P_2 (x_2 = 6.71745 mm, y_2 = 6.71745 mm, z_2= 10.0 mm) along the work plane was analysed for both healthy and defective cable which contains an air-filled void of 0.5 mm radius located at the points in the insulation bulk. The average cavity field at the cavity centre was then recorded at the instance 0.05s of the AC voltage cycle.

Equations (1) to (4) guide the principle of field distribution in a homogenous dielectric (Li *et al.*, 2024):

$$E = -\nabla V \tag{1}$$

where E is the electric field and V is the electric potential. The electric displacement in the presence of free charges can be represented as (Isa *et al.*, 2020):

$$\nabla \cdot D = \rho_v \tag{2}$$

where ρ_v represents the volume space charge density measured in C/m^3 while D is the displacement current density measured in C/m^2 and given by $D = \varepsilon E$.

The applied voltage potential V, the conductivity σ, vacuum permittivity, ε_o, and the relative permittivity, ε_r, as well as volume charge density, ρ_v are related through the Poisson's equation given in (3) (Fikri and Abdul-Malek, 2023).

$$\nabla \cdot \left[-\sigma \nabla V - \frac{\partial}{\partial t}(\varepsilon_0 \varepsilon_r \nabla V)\right] = -\frac{\rho_v}{\varepsilon} \tag{3}$$

Neglecting insulation charge density, equation (3) becomes (Wang *et al.*, 2019):

$$\nabla \cdot \left[-\sigma \nabla V - \frac{\partial}{\partial t}(\varepsilon_0 \varepsilon_r \nabla V)\right] = 0 \tag{4}$$

Equation (4) can be solved using a time-dependent study in the COMSOL Multiphysics software environment. The sinusoidal voltage U_0 is given in equation (5) (Abubakar and Zachariades, 2024; Niemeyer, 1995):

$$V = V_m \sin 2\pi f \tag{5}$$

where f is the frequency and V_m is the maximum value of the applied voltage.

The boundary condition between any two media is given in equation (6) (Sahoo and Karmakar, 2023):

$$n \cdot (\vec{D}_1 - \vec{D}_2) = \rho_s \tag{6}$$

where, ρ_s is the surface charge, while $n \cdot \vec{D}_1$ and $n \cdot \vec{D}_2$ are normal components of electric displacement of any two different mediums.

B. PD Simulation

The enhancement of electric field in and around defects within solid dielectrics leads to PD occurrence and can be modelled as streamers due to their self-sustained nature as well as measurable charge magnitude (Rodriguez-Serna et al., 2020). To initiate discharge in a defect engulfed in a solid insulation material and represent the stochastic behaviour of PDs, two invaluable conditions must be satisfied. The variations in these conditions define the extent of PD repetition rate as well as the phase at which PD events occur. The conditions are as presented in I and II below (Rodriguez-Serna et al., 2020):

I. Streamer inception criterion: the strength of the field within the void must be higher than a critical field magnitude that is enough to initiate an electron avalanche.
II. Electron generation rate criterion: a seed electron to initiate the first avalanche must be present.

PD activity is governed by the inception field and the presence of seed electron to initiate an avalanche as highlighted earlier. The PD inception field magnitude in a spherical void is given by (Musa *et al.*, 2021):

$$E_{inc} = \left(E/p\right)_{cr} \cdot p \cdot \left[1 + \frac{B}{(p d_{cav})^{1/2}}\right] \quad (7)$$

where p and d_{cav} represent the gas pressure and the diameter of the cavity respectively. The terms B and $(E/p)_{cr}$ are parameters related to gas ionization. Their respective values depend on each gas. In air, the two parameters are 8.6 $Pa^{1/2}m^{1/2}$ and 24 $VPa^{-1}m^{-1}$, respectively. The electron generation rate has two components, namely surface emission, $N_{dt}(t)$, and volume ionization, $N_{et}(t)$ given by equations (8) and (10) respectively (Borghei, Ghassemi, Rodríguez-Serna, & Albarracín-Sánchez, 2020).

$$N_{dt}(t) = N_{dt0} exp\left(-\frac{\Delta t}{\tau}\right) v_0 \cdot exp\left(-\frac{\phi_{dt} - \sqrt{eE_{cav}(t)/4\pi\varepsilon_0}}{k_b T}\right) \quad (8)$$

where e, k_b and ϕ_{dt} represent the elementary charge, Boltzmann constant and effective detrapping work function respectively. Δt is the time elapsed, in seconds, between the new PD event and the preceding one, while v_0 is the fundamental phonon frequency measured in Hz, T is the temperature in Kelvin, and τ is effective time delay constant.

The term N_{dt0} in equation (8) describes the fraction of charge carriers and is given in equation (9) (Rodríguez-Serna *et al.*, 2020):

$$N_{dt0} = \xi(q/e) \quad (9)$$

where ξ represents the proportionality factor that defines the percentage of the charge carriers responsible for the formation of de-trappable electrons and q is the true physical charge from the previous PD event.

Volume ionization involves gas particles ionization through both irradiation of energetic photons and electrons detachment from negative ions caused by the high electric field strength (Gutfleisch and Niemeyer, 1995) and is defined in terms of the radiation quantum flux density, Φ_{rad}, the pressure-reduced gas density, $(\rho/p)_0$ and effective volume of the cavity expressed as $(4/3)\,\pi r_{cav}^3$ where r_{cav} represents cavity radius. V_0 and V_i are applied voltage and PD inception voltage respectively, β_0 is the affective ionization coefficient, while C_{rad} represents the interaction between radiation and gas molecules.

The volume ionization rate can be represented by equation (10) (Gutfleisch and Niemeyer, 1995):

$$N_{et}(t) = C_{rad}\Phi_{rad}\left(\frac{\rho}{p}\right)_0 p\left(\frac{4}{3}\pi {r_{cav}}^3\right)\left(1 - \left(\frac{V_0}{V_{inc}}\right)^{-1/0.5}\right) \quad (10)$$

The net electron generation rate is therefore given by equation (11) (Niemeyer, 1995).

$$N_{net}(t) = N_{dt}(t) + N_{et}(t) \quad (11)$$

C. PD-Based Ageing Assessment

For the assessment of ageing process in the cable, sustained PD activity was simulated using COMSOL Multiphysics software environment interfaced with MATLAB software environment for a range of stressing time-based on free parameters adopted from (Callender, 2018) and (Musa *et al.*, 2023) that include the effective time decay constant (τ), the work function (Φ), the fraction of de-trappable electrons for positive and negative discharges (ξ_+/ξ_-) and the cavity pressure (p) as given in Table 3. These parameters were experimentally obtained based on the closeness of preceding PRPD measurements captured at regular intervals. The ageing process was categorized into five stages out of which only the three stages captured in Table 3 gave distinctive patterns while the last two stages are associated with insulation failure and breakdown. Based on the adopted free parameters, the cable model in this work was simulated for 50 AC cycles in each of the ageing stages and compared with those obtained by Musa *et al.*, (2023).

Table 3. Free Parameters for Cable Ageing Simulation (Callender, 2018)

Sustained PD (Hrs)	***p*** **(kPa)**	***Φ*** **(eV)**	ξ_+/ξ_-	τ **(ms)**
0.0 – 0.5	9.50	1.29	0.950	2.00
0.5 – 20.0	4.60	1.14	0.999	0.01
20.0 – 25.0	3.90	1.22	0.900	0.01

IV. RESULTS AND DISCUSSION

Electric field and electric potential distributions for healthy cable in the simulated 3D FEA model are shown in Figure 1. The simulation was performed under 11 kV, 50 Hz AC supply using a time-dependent study, and the results were recorded at 0.005 s. The average electric field has a value of 2.3809 kV/mm at the point corresponding to the void center in a defective cable. This represents a 0.76 % decrease over the 2D in (Musa *et al.*, 2021) which was recorded as 2.3991 kV/mm and a field enhancement value of 37.16 %. It can be observed from the figure that the field is maximum at the nearest point to the HV electrode while the minimum field occurs closest to the ground electrode.

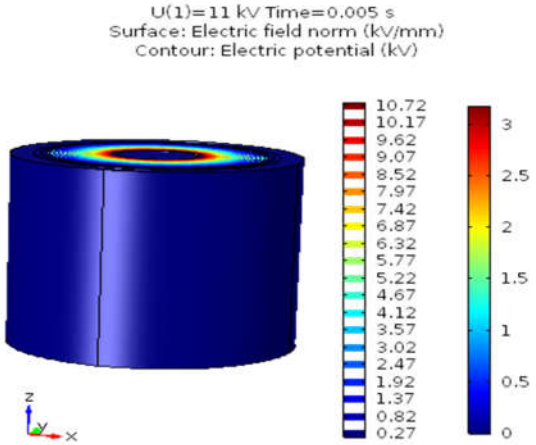

Figure 1: Electric Field and Potential Distributions in 3D for the Healthy Cable

The model was then simulated with a void of 1mm diameter, and the field behaviour was observed. The maximum field in this case occurs inside the void at the point closest to the HV electrode. The whole void has a higher field than the insulation. Field distribution was observed along the working plane before the initial PD and after it as shown in Figures 2 (a) and 2 (b) respectively. Before PD, the average cavity field was recorded as 2.9539 kV/mm, representing a 24.07 % increase over the case of a healthy cable and a 10.23% decrease when compared with the 2D model result. Table 4 shows a field magnitude comparison between the 3D model in this work and that of 2D. As shown in the table, only a small difference exists between the 2D and 3D FEA models of the same cable. However, in the presence of a cavity within the insulation, the electric field distribution in the 3D model is significantly higher than its equivalent 2D.

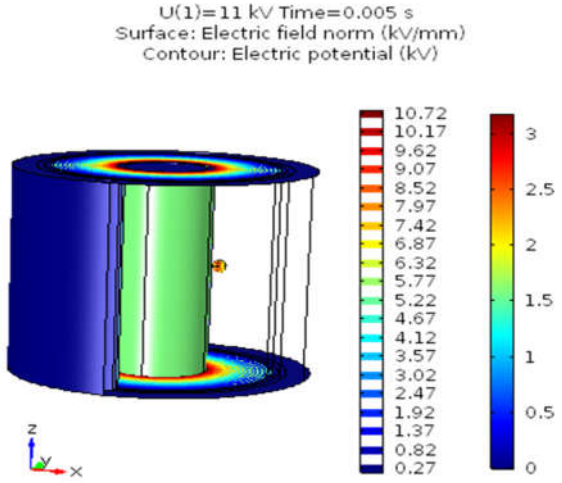

(a)

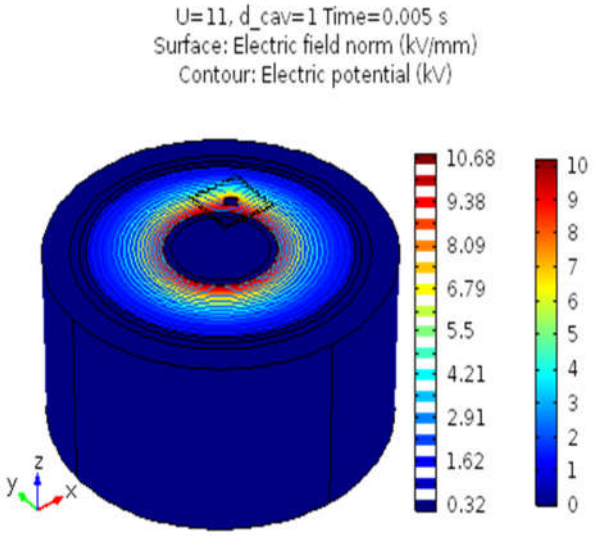

(b)

Figure 2: Electric Field and Potential Distributions in the defective Cable (a) before PD (b) after PD

Table 4: Comparison of Average Electric Field Strengths

Cable Status	Ave. Field in 2D (kV/mm)	Ave. Field 3D (kV/mm)	Diff. (%)
Healthy	2.3991	2.3809	0.76
Defective	3.2907	2.9539	10.23
Enhancement (%)	37.16	24.07	

Table 5 indicates the differences in average electric fields between defective cable (Musa *et al.*, 2021) and the 3D model in this work for an applied voltage magnitude of 11 kV at different void diameters. It can be observed from the table that the disparity between the two models is more noticeable in smaller voids. Thus, as the void size decreases, the disparity in the average field between 2D and 3D models becomes bigger. This result indicates that for smaller voids, the difference in cavity field magnitudes between 2D and 3D cable models is higher.

Table 5: Comparison of Average Field Magnitudes for Defective 2D and 3D Models at 11kV

Void Diameter (mm)	Average 2D Field (kV/mm)	Average 3D Field (kV/mm)	3D Field Decrease (%)
0.4	3.3316	2.9642	11.03
0.8	3.2999	2.9591	10.33
1.2	3.2475	2.9468	9.26
1.6	3.1755	2.9207	8.02
2.0	3.0858	2.8791	6.70

Figure 3 depicts the variation of the field along the cutline in a healthy cable where the electric field reduces from the high voltage electrode to the low voltage electrode through the

insulation material, while that of defective is depicted in Figure 4 before and after PD respectively. The void has the highest field compared to the XLPE insulation bulk before PD. After the PD event, the void experiences the lowest field. This sharp fall in magnitude of the cavity field can lead to an increased number of residual free electrons at the surface of the void, thereby causing the XLPE insulation to lose its properties and start to conduct.

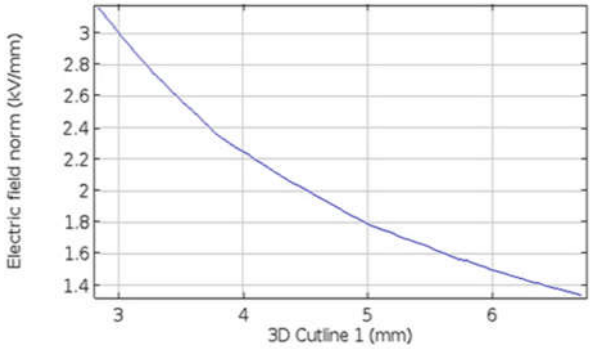

Figure 3: Line Graph for Electric Field along the Cutline for Healthy Cable

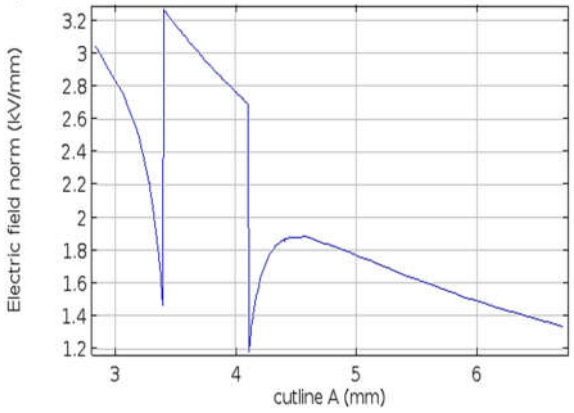

(a)

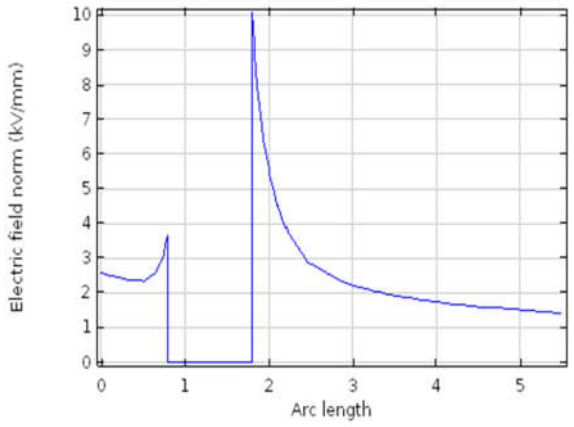

(b)

Figure 4: Line Graphs Electric Field for defective Cable (a) before PD (b) after PD

Table 6 shows the percentage decrease in the field magnitudes in this research as compared to (Musa et al., 2021). It can be observed from the table that the percentage difference in field magnitudes between the 2D and 3D models in a given void diameter is approximately equal for all values of the stressing voltages. This indicates that while void size is a significant factor in choosing of model dimension, voltage stress level for a given void size appears to indicate a little influence in the percentage field difference between the 2D and 3D models.

Table 6: Percentage Field Decrease in 3D over 2D at Different Void Sizes and Voltage Levels

Void Dia. (mm)	Percentage Field Decrease in 3D over 2D Model					
	9kV	11kV	13kV	15kV	17kV	Average
0.4	11.03	11.03	11.03	11.01	11.01	11.02
0.8	10.37	10.33	10.33	10.33	10.33	10.34
1.2	9.33	9.26	9.27	9.28	9.29	9.28
1.6	8.13	8.02	8.03	8.02	8.03	8.05
2.0	6.89	6.70	6.69	6.69	6.69	6.73

The 3D cable was further utilised for field analyses. The relationship between the diameter of the void and its average field, recorded at the void centre, under applied voltage magnitudes of 9–17 kV at intervals of 2 kV was also investigated, and the result is shown in Figure 5. It can be observed from the figure that the average field increases appreciably with an increase in the stressing voltage and decreases slightly with increasing void size.

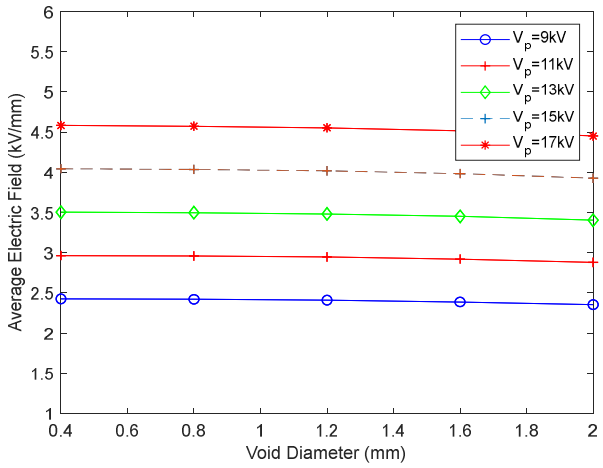

Figure 5: Impact of Void Size and Applied Voltage on Average Field

PD activity was then simulated to obtain the statistical parameters and the patterns associated with each ageing stage highlighted in Table 3. The PRPD plots corresponding to the three ageing phases considered in this paper are depicted in Figure 6 (a, b, and c).

As shown in Figure 6, the PRPD pattern exhibits a turtle-like shape in stage 1 with less variation in the PD charge magnitudes as compared to stages 2 and 3 which show rabbit-like shapes. Maximum PD charge for the three ageing stages were recorded to be 54.62 pC, 39.89 pC, and 37.39 pC for

stages 1, 2, and 3 respectively. Thus, with reference to stage 1, the PD charge decreases by 27.0 % in stage 2 and 31.5 % in stage 3. The results for each ageing stage are presented in Tables 7 to 9. The number of PDs per cycle in the first ageing stage was 9.82 and grew to 15.72 and 17.20 when the cable was continuously stressed through stages 2 and 3 respectively. Compared with stage 1, the PD repetition rate has increased by 60.08 % and 75.15 % for stages 2 and 3 respectively. This increase in PD repetition rate shows that the PD charge alone is not sufficient to predict the ageing state of the cable. The PD simulation results in this work are then compared with those obtained by Musa *et al.*, 2023 who worked on the same cable geometry represented in 2D.

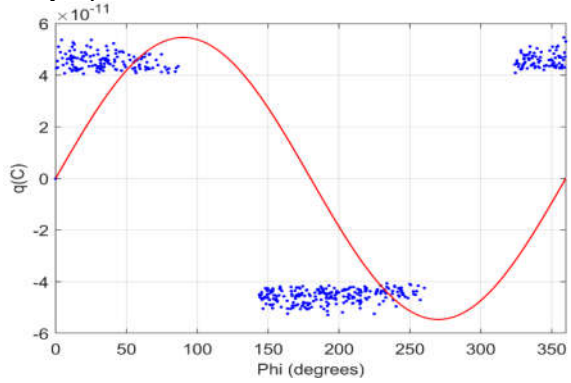

(a)

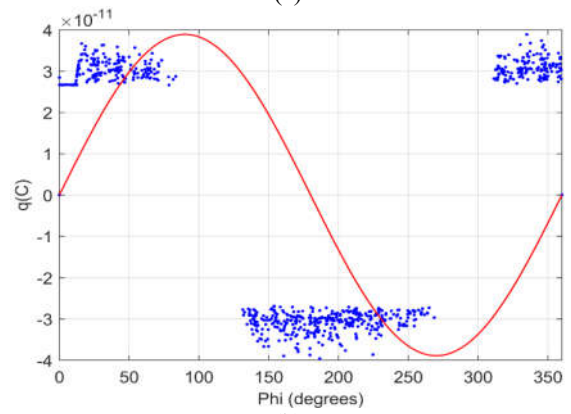

(b)

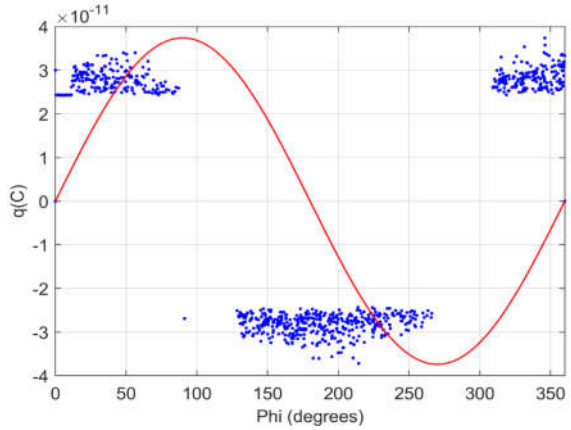

(c)

Figure 6: PRPD Patterns for Ageing Progress of the XLPE Cable for a Void Diameter of 1.0 mm for 50 AC voltage cycles (a) Stage (b) Stage 2 (c) Stage 3

Figure 7 (a, b, and c) depicts PD pulses as well as cavity field variation for one cycle in each of the three ageing phases. It can be observed that more PD activity takes place in stage 3, and the least occurs in stage 1 as illustrated by the pulses.

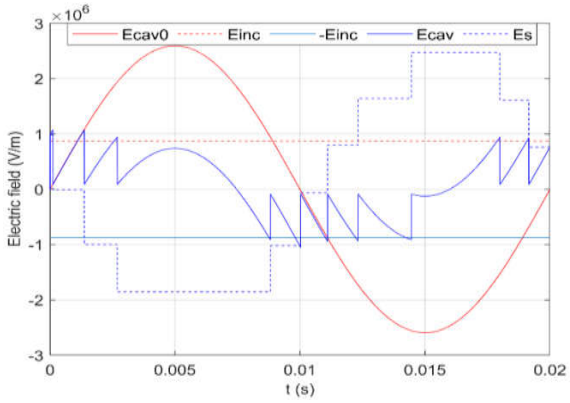

(a)

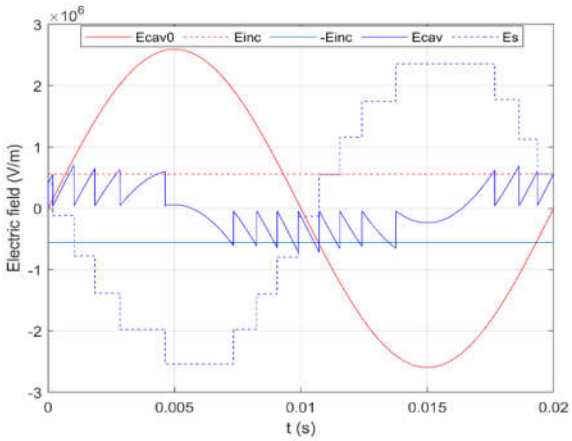

(b)

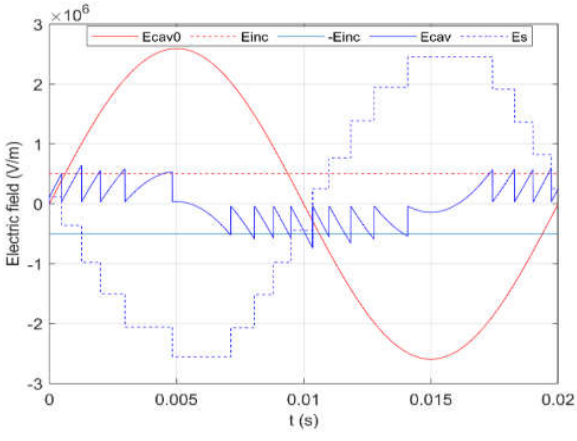

(c)

Figure 7: Electric Fields in one ac cycle for Void Diameter of 1.0 mm (a) Stage 1 (b) Stage 2 (c) Stage 3

It can be inferred from Table 7 that maximum and mean PD charges are both higher in the 2D model, while the 3D model has a higher minimum charge of 1.33 %. The difference is however highest in average mean charge magnitude which

is the main parameter of interest. The number of PD occurrences per cycle is higher in the 3D model than that of the PD. Hence, while the PD charge magnitudes in the 3D cable model are lower, more activity is taking place in every AC cycle of the stressing voltage which will cause the insulation to experience a more sustained PD that can lead to accelerated ageing. The inception and extinction fields were found to be equal in both models at stages 2 and 3 which can be associated with the cable geometry, void size, and location as well as the parameters involved in the computations.

Table 7: PD Simulation Statistical Parameters for Ageing Stage 1

Reference	**Geometry**	E_{inc} **(kV/m)**	E_{ext} **(kV/m)**	q_{max} **(pC)**	q_{mean} **(pC)**	q_{min} **(pC)**	***PD/cycle***
Musa *et al*.,2023	2D	1070.30	1188.80	57.73	50.17	40.02	7.81
This work	3D	817.37	86.21	54.62	45.52	40.55	9.82
Percentage increase/decrease		23.63	92.75	5.38	9.27	1.33	25.74

In Table 8, a similar comparison of the PD simulation parameters for 2D and 3D models of the same cable is presented. In this phase, the percentage difference in terms of PD charges between the two models widens when compared to stage 1. In this phase, the difference in the maximum, mean and minimum PD charge magnitudes in the 3D is less than that of the corresponding 2D model by 31.39%, 39.67%, and 33.41 % respectively. The difference in PD charge per cycle however reduced from 25.74% in stage 1 to 2.26% in stage 2.

Table 8: PD Simulation Statistical Parameters for Ageing Stage 2

Reference	**Geometry**	E_{inc} **(kV/m)**	E_{ext} **(kV/m)**	$\mathbf{q}_{max}$ **(pC)**	q_{mean} **(pC)**	q_{min} **(pC)**	***PD/cycle***
Musa et al.,2023	2D	557.69	41.75	58.14	50.62	40.01	15.47
This work	3D	557.69	41.75	39.89	30.54	26.64	15.82
Percentage increase/decrease		0.00	0.00	31.39	39.67	33.41	2.26

In the third stage which is the closest to the breakdown phase of the cable, the extinction and extinction field magnitudes are equal in both 2D and 3D models of the cable. Like the preceding two ageing phases, the PD charge magnitudes are lower in the 3D model while the PD repetition rate increases from 16.98 to 17.31, representing 1.94 % as shown in Table 9.

Table 9: PD Simulation Statistical Parameters for Ageing Stage 3

Reference	Geometry	E_{inc} (kV/m)	E_{ext} (kV/m)	q_{max} (pC)	q_{mean} (pC)	q_{min} (pC)	*PD/cycle*
Musa et al.,2023	2D	505.38	35.39	63.17	53.15	40.00	16.98
This work	3D	505.38	35.39	37.39	27.95	24.27	17.31
Percentage increase/decrease		0.00	0.00	40.81	47.41	39.33	1.94

V. CONCLUSION

The Electric field analysis was performed in a healthy and defective cable model simulated using the FEA approach for different cavity sizes. The results were compared with those obtained from a corresponding 2D cable. A close agreement was observed for healthy cable, however, there is a significant reduction in the electric field magnitude of a 3-dimensional defective cable compared to the 2D for various cavity radii. For any given cavity radius, the average field increases with an increase in applied voltage stress. Also, the cavity field under a given voltage decreases with increasing cavity size. Thus, while a 2-dimensional model will suffice in the electric field analysis of a healthy cable, a significant difference in field magnitude exists between 2D and 3D models when a void is present within the insulation bulk.

PD behaviour was simulated for three ageing phases of the cable based on adopted free parameters obtained from experiment. The streamer inception and extinction fields remain the same in both 2D and 3D models. The PD charge magnitudes in the 3-dimensional model were generally lower than those in the 2D in all the three ageing stages considered in this work. However, the number of PDs per cycle is higher in the 3D model by 25.74 %, 2.26 %, and 1.94 % in stages 1, 2, and 3 respectively.

AUTHOR CONTRIBUTIONS

S. H. Sulaiman: Conceptualization, Methodology, Software Simulation, Writing – original draft, Writing – review & editing. **A. Abdulkarim**: Conceptualization, Methodology, Writing original draft, Writing – review & editing. **A. S. Abubakar**: Writing – review & editing. **G. S. Shehu**: Writing – review & editing. **U. Musa**: Conceptualization, Methodology, Software Simulation. **A. A. Mas'ud**: Software Simulation.

REFERENCES

Abubakar, A., and Zachariades, C. (2024). Phase-Resolved Partial Discharge (PRPD) Pattern Recognition Using Image Processing Template Matching. Sensors, 24 (11): 1-15.

Aliyu, B. D., Rohani, M. N. K. H., Musa, U., Jibril, Y., Sulaiman, S. H., Mas'ud, A. A. and Muhammad-Sukki, F. (2023). The Impact of Cavity Size on Electric Field Distribution and PD Inception Voltage in Epoxy-resin Insulation. Paper presented at the 2023 IEEE 3rd International Conference in Power Engineering Applications (ICPEA): 229-232.

Arikan, O., Uydur, C. C., and Kumru, C. F. (2023). Insulation evaluation of MV underground cable with partial discharge and dielectric dissipation factor measurements. Electric Power Systems Research, 220: 109338.

Bessissa, L., Boukezzi, L., Mahi, D., Boubakeur, A., and Distribution. (2017). Lifetime estimation and diagnosis of XLPE used in HV insulation cables under thermal ageing: arithmetic sequences optimised by genetic algorithms approach. IET Generation, Transmission 11 (10): 2429-2437.

Borghei, M., Ghassemi, M., Rodríguez-Serna, J. M., and Albarracín-Sánchez, R. (2020). A Finite Element Analysis and an Improved Induced Charge Concept for Partial Discharge Modeling. IEEE Transactions on Power Delivery, 36 (4): 2570-2581.

Boudiaf, A., Bouazabia, S., Harid, N., and Amrani, M. (2022). Analytic calculation of partial discharge threshold in a gaseous cavity within high voltage cable insulation. Electrical Engineering, 104 (2): 555-565.

Callender, G. (2018). Modelling partial discharge in gaseous voids. PhD Thesis, University of Southampton, United Kingdom.

Choudhary, M., Shafiq, M., Kiitam, I., Hussain, A., Palu, I., and Taklaja, P. (2022). A review of ageing models for electrical insulation in power cables. Energies, 15(9): 1-20.

Choudhary, M., Shafiq, M., Kiitam, I., Palu, I., Hassan, W., and Singh, P. P. (2024). Investigation of partial discharge characteristics in XLPE cable insulation under increasing electrical stress. Engineering Failure Analysis, 108006.

Dmitriev, V., Oliveira, R. M., Zampolo, R. F., Moutinho de Vilhena, P. R., de Souza Brasil, F., and Fernandes, M. F. (2023). Partial Discharges: Physics and Classification. In Partial Discharges in Hydroelectric Generators: Detection, Processing, Classification, and Pinpointing (pp. 11-36): Springer.

Fikri, M., and Abdul-Malek, Z. (2023). Partial discharge diagnosis and remaining useful lifetime in XLPE extruded power cables under DC voltage: a review. Electrical Engineering, 105 (6): 4195-4212.

Gutfleisch, F., and Niemeyer, L. (1995). Measurement and simulation of PD in epoxy voids. IEEE Transactions on Dielectrics, 2(5): 729-743.

Illias, H., Chen, G., and Lewin, P. L. (2011). Modelling of Partial Discharge Activity in Spherical Cavities Within a Dielectric Material. IEEE electrical insulation magazine, 27(1): 38-45.

Illias, H., Chen, G., and Lewin, P. L. (2012). Partial discharge within a spherical cavity in a dielectric material as a function of cavity size and material temperature. IET Science, Measurement and Technology, 6(2): 52-62.

Illias, H., Yuan, T. S., Mokhlis, H., Chen, G., and Lewin, P. L. (2012). Partial discharge patterns in high voltage insulation. Paper presented at the 2012 IEEE International Conference on Power and Energy (PECon): 750-755.

Isa, M. A. M., Rohani, M. N. K. H., Rosmi, A. S., Isa, M., Rosle, N., Mustafa, W. A., Daniel, I. N. and Roslan, M. A. (2020). Investigation on partial discharge activities in cross-linked polyethylene power cable using finite element analysis. Paper presented at the Journal of Physics: Conference Series, 1432 (1), 012024.

Khouildi, E., Attia, R., and Chtourou, N. (2016). Numerical modeling of the electric field and the potential distributions in heterogeneous cavities inside XLPE power cable insulation. Journal of Electrical and Electronics Engineering, 9(2): 37-42.

Li, Y., Zhen, G., Liu, Y., Song, H., Liang, Y., Liu, X., Shaoxin,M., Li, S. (2024). Effect of temperature on partial discharges activity and electrical trees propagation in XLPE. IET Science, Measurement and Technology 18(6): 300-309.

Liu, F., Huang, X., Wang, J., and Jiang, P. (2012). Insulation ageing diagnosis of XLPE power cables under service conditions. Paper presented at the 2012 IEEE International Conference on Condition Monitoring and Diagnosis: 647-650.

Mas'ud, A. A., Musa, U., Sulaiman, S. H., Shehu, I. A., and Aliyu, B. D. (2022). Partial discharge detection and classification: implications on the power industry. Paper presented at the Proc. 18th International Conference and Exhibition on Power and Telecommunications (ICEPT), 146-152.

Mirshekali, H., Mortensen, L. K., and Shaker, H. R. (2024). Reliability-aware multi-objective approach for predictive asset management: A Danish distribution grid case study. Applied Energy, 358, 122556.

Musa, U., Mati, A. A., Mas' ud, A. A., Shehu, G. S., Albarracin-Sanchez, R., and Rodriguez-Serna, J. M. (2021). Modelling and analysis of electric field variation across the insulation system of an MV power cable. Paper presented at the 2021 International Conference on Electrical, Communication, and Computer Engineering (ICECCE), 1-5

Musa, U., Mati, A. A., Mas'ud, A. A., Shehu, G. S., Rodríguez-Serna, J. M., Al-Shammari, S. J., Rohani, M.N.K.H. and Muhammad-Sukki, F. (2023). FEA-Based Simulation of Accelerated Ageing in a Power Cable Due to Sustained Partial Discharge Activities in a Spherical Cavity. Arabian Journal for Science Engineering: 1-15.

Niemeyer, L. (1995). A generalised approach to partial discharge modelling. IEEE Transactions on Dielectrics and Electrical Insulation, 2 (4): 510-528.

Polyakov, D. A., Yurchuk, D. A., and Nikitin, K. I. (2018). Cables XLPE-insulation Residual Life Monitoring. Paper presented at the 2018 IEEE International Conference on High Voltage Engineering and Application (ICHVE), 1-4.

Rodríguez-Serna, J. M., Albarracín-Sánchez, R., and Mas' ud, A. A. (2020). Finite-element-analysis models for

numerical simulation of partial discharges in spherical cavities within solid dielectrics: a review and a novel method. High Voltage, 5(5): 556 - 568. doi:10.1049/hve.2019.0392

Sahoo, R., and Karmakar, S. (2023). Investigation of electrical tree growth characteristics and partial discharge pattern analysis using deep neural network. Electric Power Systems Research, 220, 1-10.

Uydur, C. C., Arikan, O., and Kalenderli, O. (2018). The Effect of insulation defects on electric field distribution of power cables. Paper presented at the 2018 IEEE International Conference on High Voltage Engineering and Application (ICHVE), 1-4, Greece: IEEE.

Wang, J., Li, P., Deng, X., Li, N., Xie, X., Liu, H., and Tang, J. (2019). Evaluation on partial discharge intensity of electrical equipment based on improved ANFIS and ultraviolet pulse detection technology. IEEE Access, 7 (2019): 126561-126570.